Weak Form Equation-Based Finite Element Modeling of Viscoelastic Asphalt Mixtures[1]

Yuqing Zhang, Ph.D. A.M. ASCE

Lecturer

School of Engineering and Applied Science, Aston University

Aston Triangle, Birmingham, B4 7ET, U.K.

Phone: +44(0)121 204 3391, Email: y.zhang10@aston.ac.uk

Bjorn Birgisson, Ph.D., P.E.

Executive Dean, School of Engineering and Applied Science, Aston University

Aston Triangle, Birmingham, B4 7ET, UK

Phone: +44(0)7825 125908, Email: bjorn.birgisson@aston.ac.uk

Robert L. Lytton, Ph.D., P.E., F. ASCE

Professor, Fred J. Benson Chair

Zachry Department of Civil Engineering

Texas A&M University

3136 TAMU, CE/TTI Bldg. 503A, College Station, Texas 77843

Phone: (979) 845-9964, Email: r-lytton@civil.tamu.edu

[1] This is an Accepted Manuscript of an article published by *ASCE* in *Journal of Materials in Civil Engineering*. The final publication is available online via http://dx.doi.org/10.1061/(ASCE)MT.1943-5533.0001395

Abstract

The objective of the study is to demonstrate using weak form partial differential equation (PDE) method for a finite element (FE) modeling of a new constitutive relation without the need of user subroutine programming. The viscoelastic asphalt mixtures were modeled by weak form PDE based FE method as the examples in the paper. A solid-like generalized Maxwell model was used to represent the deforming mechanism of a viscoelastic material, the constitutive relations of which were derived and implemented in the weak form PDE module of Comsol Multiphysics, a commercial FE program. The weak form PDE modeling of viscoelasticity was verified by comparing Comsol and Abaqus simulations, which employed the same loading configurations and material property inputs in virtual laboratory test simulations. Both produced identical results in terms of axial and radial strain responses. The weak form PDE modeling of viscoelasticity was further validated by comparing the weak form PDE predictions with real laboratory test results of six types of asphalt mixtures with two air void contents and three aging periods. The viscoelastic material properties such as the coefficients of a Prony series model for the relaxation modulus were obtained by converting from the master curves of dynamic modulus and phase angle. Strain responses of compressive creep tests at three temperatures and cyclic load tests were predicted using the weak form PDE modeling and found to be comparable with the measurements of the real laboratory tests. It was demonstrated that the weak form PDE based FE modeling can serve as an efficient method to implement new constitutive models and free engineers from user subroutine programming.

Keywords: Asphalt mixture, viscoelasticity, finite element modeling, weak form PDE, master curve, generalized Maxwell model

Introduction

As a viscoelastic material, an asphalt mixture exhibits a time and frequency dependent behavior. The current stress or strain responses of the asphalt mixtures are affected by the whole history of the strain or stress inputs prior to the current time. Temperature has a significant influence on the material responses, which is commonly accounted for by modulus master curves and time-temperature shift functions. Extensive studies were performed to determine the appropriate shift functions and to develop the master curve models for dynamic modulus and phase angle of asphalt mixtures (Pellinen et al. 2002; Biligiri et al. 2010; Zhang et al. 2012a; Zhao et al. 2012). The dynamic modulus has become a major input for material properties in the Mechanical-Empirical Pavement Design Guide (MEPDG) (ARA 2004). Relaxation modulus and creep compliance are also employed to characterize the viscoelastic properties of the asphalt mixtures, especially in a viscoelastic constitutive modeling (Gibson et al. 2003; Zhang et al. 2012b). Theoretically, all viscoelastic variables including complex modulus (dynamic modulus as its magnitude), complex compliance, relaxation modulus and creep compliance are interconvertible. Studies were also presented in the literature to introduce these conversions for use in practice (Park and Schapery 1999; Mun et al. 2007; Katicha et al. 2008; Hu and Zhou 2010).

The viscoelasticity of asphalt mixtures has been well characterized by viscoelastic theories and laboratory tests as shown in the aforementioned studies in the literature. However, applying viscoelastic models and theories in material performance predictions and pavement structural analysis are limited due to some implementation difficulties. For instance, in the pavement research community, Abaqus is one of the commonly-used finite element (FE) analysis programs that are utilized to model asphalt mixtures' performance and simulate pavement structures (Huang et al. 2011; Darabi et al. 2012; Zhu and Sun 2013). Nevertheless, the following limitations restrict the FE modeling of asphalt mixtures in Abaqus.

1) The existing viscoelasticity module cannot be used with any of the existing plasticity or damage modules in Abaqus (ABAQUS 2010). A user material subroutine must be programmed in order

to simultaneously address different material mechanisms such as viscoelasticity, plasticity, fracture, damage and their coupling effects.

2) The time-temperature shift factor can only defined as the Williams–Landel–Ferry (WLF) and Arrhenius functions (supported as Input File mode only). A user defined time-temperature shift factor must be coded using user subroutine programs.
3) Programming a user defined subroutine requires extensive experience with mastering the computer programming language, which distracts the pavement researchers' attention from the material constitutive modeling and narrows the pavement structural simulations.
4) The users need to spend significant efforts to debug the user defined subroutines to avoid potential computational errors and issues such as non-convergence, circular dependency, low-efficiency iteration, etc.

For other numerical programs developed by pavement researchers, similar problems still exist with additional issues such as non-user-friendly interfaces, limited modeling abilities and restrictions on specific constitutive models. A robust FE modeling method is needed to free pavement researchers from the numerical issues and simultaneously allow them to try their own material constitutive models in an efficient way in pavement analysis. The weak form partial differential equation (PDE) based FE modeling is the tool that can achieve the objective. Therefore, the objective of the paper is to demonstrate how a constitutive relation is modeled by the weak form PDE method and implemented in a finite element program without a need of user subroutine programming. The PDE based viscoelastic modeling of an asphalt mixture is demonstrated as an example in this paper to show how this can be done.

From a physics perspective, elasticity, viscoelasticity, plasticity, and fracture are different aspects of mechanical physics that may occur simultaneously in a material. The control or constitutive equations of these physics can be derived by thermodynamics using the virtual work principle and represented as ordinary differential equations (ODE) or partial differential equations (PDE) (ODE is treated as a special PDE). Thus different physics can be modeled simultaneously and evaluated for their interactions by solving the PDEs at one time. The weak form of a PDE is regarded as a generalization of the virtual work

principle and is an important mathematical analysis method to find the solutions to the PDE. More explanations of the weak form of the PDE is presented in the section "Weak Form PDE Modeling of Viscoelasticity" of this paper, in which a structural analysis method is introduced to explain the concept of weak form PDE.

As a general-purpose FE program, Comsol Multiphysics provides an efficient computational platform to solve weak form PDEs and to address the coupling effects of different physics (COMSOL 2013a). The major advantage of using the weak form of PDE modeling in Comsol rather than traditional FE modeling is that no user subroutine is needed and the control/constitutive equations of different physics can be defined and solved by equation based models such as weak form PDEs. Thus the different physics such as viscoelasticity, plasticity, fracture, heat transfer and moisture diffusion can be easily modeled using weak form PDEs. Their interactions and coupling effects can also be evaluated.

This paper is focused on viscoelastic modeling using the weak form PDE in Comsol and asphalt mixtures are selected as the viscoelastic materials to be tested for model calibration and validation. The next section presents the asphalt mixture materials and laboratory tests. Master curves of dynamic modulus and phase angle are constructed for six different asphalt mixtures. Then linear viscoelastic constitutive relations are introduced and relaxation modulus is determined using dynamic modulus and phase angle master curves. After that, weak form PDE modeling of viscoelasticity is presented based on a solid-like generalized Maxwell model. The weak form PDE modeling of viscoelasticity is verified by comparing the predictions with Abaqus results and is further validated by comparing the predictions with laboratory test results. The last section presents the summary and conclusions.

Laboratory Testing and Master Curves of Asphalt Mixtures

The objectives of laboratory testing are 1) to determine the viscoelastic properties of asphalt mixtures which are used as inputs to the weak form PDE based FE modeling; and 2) to validate the weak form PDE based modeling of viscoelasticity in the Comsol program.

Materials and Experiments

Laboratory tests were performed on lab-mixed-lab-compacted (LMLC) asphalt mixtures that were fabricated with one asphalt binder, at two air void contents and three aging periods. Three replicate specimens were fabricated for each combination of the variables. The testing protocol (including test method, loading parameters, and temperatures), materials and measurements are summarized in Table 1.

As for the materials used in the tests, a commonly-used Texas Hanson limestone was selected in this study and the gradation of the aggregates was determined based on a Type C (coarse surface) dense gradation specified by the Texas Department of Transportation (TxDOT) (2004). The optimum asphalt content was calculated based on the TxDOT test procedure (TxDOT 2008) and was determined as 4.4%. The asphalt concrete specimens were compacted using the Superpave gyratory compactor to a cylindrical sample with 150 mm in diameter and 175 mm in height. Then the asphalt concrete samples were cored to 100 mm in diameter and cut to 150 mm in height. The target air void contents had two levels including 4% and 7%. Some of the asphalt concrete specimens were tested once they were fabricated, while some of the specimens were stored in the aging room and aged at a constant temperature of 60°C for 3 months and 6 months, respectively. Before testing, the specimens were put in an environmental chamber at the testing temperature for at least 3 hours to reach the equilibrium temperature. Then they were tested using a Universal Testing Machine (UTM) based on the test plan shown in Table 1.

It is noted that the test results of dynamic modulus tests including dynamic modulus and phase angle are used to construct the master curves which are then employed to determine the viscoelastic properties such as relaxation moduli and used as the inputs to the FE modeling. The test results of creep tests and cyclic load tests are used to compare with the FE modeling predictions so as to validate the equation-based FE modeling of the viscoelasticity.

Dynamic Modulus Tests and Master Curve Constructions

Compressive dynamic modulus tests were performed at six frequencies and four temperatures as indicated in Table 1. To ensure linear viscoelastic behavior of the material, different stress magnitudes were used in each level of temperature and frequency to limit the dynamic strains to less than 150 με which is recognized as the strain limit for the linear viscoelastic asphalt mixture under a compressive load

(Levenberg and Uzan 2004). Same criterion was used in determining the load levels in other laboratory tests. Trial tests were performed on dummy samples to determine the stress levels and ensure the strain limit is maintained. It basically requires lower stresses being applied at the lower frequencies and higher temperatures or for the asphalt mixtures with higher air void content and shorter aging period, as shown in Table 1. The dynamic modulus and phase angle were measured using the built-in algorithm in the UTM data acquisition and analysis program.

In linear viscoelastic theory, the complex modulus is used to characterize the constitutive behavior of the viscoelastic materials when subjected to a stress or strain oscillation. The magnitude of the complex modulus is termed the dynamic modulus and the phase lag between stress and strain is the phase angle. The complex modulus is expressed as

$$E^*(\omega) = E'(\omega) + iE''(\omega) = \left|E^*(\omega)\right|(\cos\varphi + i\sin\varphi) \tag{1}$$

where $E^*(\omega)$ is the complex modulus, $E'(\omega)$ and $E''(\omega)$ are the storage modulus and loss modulus which are the real part and imaginary part of the complex modulus, $\left|E^*(\omega)\right|$ is the dynamic modulus, φ is the phase angle, $i = \sqrt{-1}$, ω is angular frequency in rad/sec, $\omega = 2\pi f$ and f is the loading frequency in Hz. Typical results of the dynamic modulus and phase angle measurements are shown in Fig 1 and Fig 2, respectively. Based on the measurements at different temperatures and loading frequencies, the master curves of dynamic modulus and phase angle can be constructed according to the time–temperature superposition principle. The master curve model for dynamic modulus employs a sigmoidal function as below (Pellinen et al. 2002; ARA 2004).

$$\log\left(\left|E^*\right|\right) = \delta + \frac{\alpha}{1 + e^{\eta - \gamma\log(f_r)}} \tag{2}$$

where $\left|E^*\right|$ is the dynamic modulus, δ is the minimum logarithm of the dynamic modulus, α is span of the logarithm of the dynamic modulus, η and γ are shape parameters, f_r is reduced frequency in Hz that has $f_r = f \cdot a_T$, where f is the loading frequency in Hz, a_T is a time-temperature shift factor

shown as below which employs a polynomial fitting function as the high temperature data are included (Francken and Verstraeten 1998; Biligiri et al. 2010).

$$\log(a_T) = aT^2 + bT + c \tag{3}$$

where T is the temperature in Kelvin and a, b, and c are fitting parameters.

The master curve model for the phase angle is a β -model developed by the authors (Zhang et al. 2012a) which allows a non-symmetric bell-shaped master curve on the log-log plot of the phase angle versus the frequency. The β -model is presented as:

$$\varphi = \frac{\varphi_{max}}{Exp\left\{\left(1+\frac{1}{\beta}\right)\left[\left(\frac{f_0}{f_r}\right)^{\beta}-1\right]\right\}\left(\frac{f_r}{f_0}\right)^{\beta+1}} \tag{4}$$

where φ_{max} is the maximum phase angle, f_0 is the reference frequency at which φ_{max} occurs, β is a fitting parameter that determines the curvature of the phase angle master curve; f_r is reduced frequency in Hz that has $f_r = f \cdot a_T$, where f is the loading frequency in Hz and a_T is a time-temperature shift factor that uses the same formulation as in Eq. 3 (Biligiri et al. 2010).

Eqs. 2 and 4 allow for the use of Excel spreadsheets and the Solver function to construct the master curves of dynamic modulus and phase angle. The Solver function performs nonlinear least square regression in Excel spreadsheets to determine the model coefficients in Eqs. 2, 3 and 4. Examples are given for the master curves of the dynamic modulus and phase angle in Fig. 1 and Fig. 2, respectively. Table 2 summarizes the master curve model coefficients for dynamic modulus and phase angle of the six types of asphalt mixtures with different air void contents and aging periods. It is noted that, to construct better master curves (e.g., with higher R^2 values as indicated in Figs. 1 and 2), different a_T values were determined for dynamic modulus and phase angle, respectively. The curves in Figs. 1 and 2 that are marked as “master curve” are the fitted dynamic modulus laboratory data using master curve models; the

curves labeled as "predicted" are those predicted from the relaxation modulus modeled by Prony series as explained in the subsequent section.

Constitutive Relations and Relaxation Modulus of Asphalt Mixtures

The linear viscoelastic constitutive relations are firstly presented in terms of relaxation modulus for one-dimensional condition and using relaxation bulk and shear moduli for multi-axial condition. Then Prony series model coefficients of the relaxation modulus are determined based on dynamic modulus and phase angle master curves.

Linear Viscoelastic Constitutive Relations

The constitutive relations for a linear viscoelastic material are generally expressed as volumetric and deviatoric components of stress and strain tensors. Under multi-axial states of stress, the constitutive relations are presented as (Findley et al. 1989):

$$\sigma_{kk} = 3\int_0^t K\left(t-\xi\right)\frac{\partial \varepsilon_{kk}}{\partial \xi}d\xi \tag{5}$$

$$s_{ij} = 2\int_0^t G\left(t-\xi\right)\frac{\partial e_{ij}}{\partial \xi}d\xi \tag{6}$$

where $\sigma_{kk} = \sigma_{11} + \sigma_{22} + \sigma_{33}$ is the first invariant of stress tensor which is the volumetric component of stress, $\varepsilon_{kk} = \varepsilon_{11} + \varepsilon_{22} + \varepsilon_{33}$ is the volumetric strain, $K\left(t\right)$ is the relaxation bulk modulus, $s_{ij} = \sigma_{ij} - 1/3\,\sigma_{kk}\delta_{ij}$ is the deviatoric stress tensor and δ_{ij} is the Kronecker delta, $e_{ij} = \varepsilon_{ij} - 1/3\,\varepsilon_{kk}\delta_{ij}$ is the deviatoric strain tensor, $G\left(t\right)$ is the relaxation shear modulus, t is the current time of interest, and ξ is an integration variable that is a time before current time.

Under a uniaxial state of stress, the constitutive relation is expressed as:

$$\sigma_{ij} = \int_0^t E\left(t-\xi\right)\frac{\partial \varepsilon_{ij}}{\partial \xi}d\xi \tag{7}$$

where σ_{ij} and ε_{ij} are the stress tensor and strain tensor, respectively. $E(t)$ is the relaxation modulus. If a solid-like generalized Maxwell model is used, $E(t)$ can be characterized by a Prony series model:

$$E(t) = E_{\infty} + \sum_{m=1}^{M} E_m \exp\left(-\frac{t}{\tau_m}\right) \tag{8}$$

where E_{∞} is a long term equilibrium modulus; E_m are components of the relaxation modulus; τ_m are components of relaxation time; and *M* is the total number of the Maxwell elements (one Maxwell element is composed of one elastic spring and one viscous dashpot connected in series).

Similarly, the relaxation bulk modulus and shear modulus can also be expressed by a Prony series model as below:

$$K(t) = K_{\infty} + \sum_{m=1}^{M} K_m \exp\left(-\frac{t}{\tau_m^K}\right) \tag{9}$$

$$G(t) = G_{\infty} + \sum_{m=1}^{M} G_m \exp\left(-\frac{t}{\tau_m^G}\right) \tag{10}$$

where K_{∞} and G_{∞} are the long term equilibrium bulk modulus and shear modulus, respectively; K_m and G_m are components of the relaxation bulk and shear modulus, respectively; τ_m^K and τ_m^G are relaxation times for the bulk and shear responses, respectively, and it is normally assumed that $\tau_m^K = \tau_m^G = \tau_m$.

The relationships between $K(t)$, $G(t)$ and $E(t)$ can be established by a convolution integral using a time dependent Poisson's ratio (e.g., $\upsilon(t)$) which is also a material property for viscoelastic materials. The laboratory measuring and viscoelastic modeling of the time dependent Poisson's ratio for asphalt concrete can be found in the literature (Zhang et al. 2012a; Zhang et al. 2014). To simplify the analysis, a constant Poisson's ratio was assumed for the material, and one can have (Wineman and Rajagopal 2001):

$$K(t) = \frac{E(t)}{3(1-2\upsilon_0)} \tag{11}$$

$$G(t) = \frac{E(t)}{2(1+\upsilon_0)} \tag{12}$$

where υ_0 is the Poisson's ratio that is assumed as a constant in this study. Based on Eqs. 11 and 12, K_∞, G_∞, K_m, G_m, τ_m can be calculated once $E(t)$ and υ_0 are known. In this study, the values of Poisson's ratio for the six asphalt mixtures are obtained from the authors' previous study (Zhang et al. 2014) and the data are shown in Table 3.

Determination of Relaxation Modulus Based on Dynamic Modulus Test Results

In the pavement community, the dynamic modulus test has become a standard test, e.g., simple performance test, to characterize the viscoelastic performance of asphalt mixtures (Witczak et al. 2002) and the results of dynamic modulus have been used as a major input to the MEPDG (ARA 2004). However, the relaxation modulus is more widely used in the performance prediction of asphalt concrete, such as in the finite element (FE) simulations and other computational programs. Thus it is convenient to determine the relaxation modulus based on the dynamic modulus test results, which have been extensively studied in the literature as discussed in the Introduction.

To determine the coefficients of the relaxation modulus in Eq. 8 based on the dynamic modulus test results, the following two relationships are commonly used:

$$E'(\omega) = E_\infty + \sum_{i=1}^{M} \frac{\omega^2 \tau_m^2 E_m}{1+\omega^2 \tau_m^2} \tag{13}$$

$$E''(\omega) = \sum_{i=1}^{M} \frac{\omega \tau_m E_m}{1+\omega^2 \tau_m^2} \tag{14}$$

Then the dynamic modulus and phase angle are determined as below:

$$\left|E^*(\omega)\right| = \sqrt{\left[E'(\omega)\right]^2 + \left[E''(\omega)\right]^2} \tag{15}$$

$$\varphi = \tan^{-1}\left[\frac{E''(\omega)}{E'(\omega)}\right] \tag{16}$$

Based on the master curves of the dynamic modulus and phase angle as constructed using Eqs. 2, and 4, one can determine the Prony model coefficients of the relaxation modulus, i.e., E_∞, E_m and τ_m by minimizing the error between the master curve values and the predictions using Eqs. 13 to 16. Note that, in this study, τ_m was controlled varying from 10^{-6} to 10^4 s which covered the range of the relaxation time obtained from time-temperature shifting, thus only E_∞ and E_m were used as the regression coefficients. The dashed lines in Figs 1 and 2 show the examples for the dynamic moduli and phase angles predicted using the relaxation modulus Prony model. Similar figures to Figs 1 and 2 were also obtained for the other five asphalt mixtures, but not shown in the paper due to the length of the paper. The regressed relaxation modulus coefficients for the six asphalt mixtures are summarized in Table 3, which basically indicates a higher modulus (take instantaneous modulus, for example) as the asphalt mixture has a lower air void content or a longer aging period.

It is noted that in this study, the dynamic modulus and phase angle were both utilized in the formulation of the regression minimization objective (as shown in Eq. 17) considering the fact that both dynamic modulus and phase angle are the two non-negligible components of the complex modulus. Using only one component of complex modulus may not accurately represent the viscoelastic properties of the material. It is also noted that Eq. 17 normalizes the two regression variables, i.e., dynamic modulus and phase angle, to avoid the influences of the different unit and magnitude of the regression variables on the regression objectives (i.e., the error) so that the two different variables can be accounted for in a single regression formulation. The similar regression techniques were also employed in the literature (Levenberg and Shah 2008; Zhao et al. 2013).

$$error = \frac{1}{N}\left[\sum_{i=1}^{N}\left(1-\frac{\left|E^*(\omega_i)\right|_{Predicted}}{\left|E^*(\omega_i)\right|_{MasterCurve}}\right)^2+\sum_{i=1}^{N}\left(1-\frac{\varphi(\omega_i)_{Predicted}}{\varphi(\omega_i)_{MasterCurve}}\right)^2\right] \quad (17)$$

Weak Form Equation-Based FE Modeling of Viscoelasticity

The stress and strain relations are derived for a solid-like generalized Maxwell model to represent the viscoelastic behavior of the material. Then weak form PDE is introduced and implemented step by step in Comsol to solve the viscous strains and predict the viscoelastic stress responses.

Stress and Strain Analysis in Generalized Maxwell Model

The mechanical analogs of the Prony series model (i.e., Eqs. 8, 9 and 10) can be represented by a solid-like generalized Maxwell model which has one spring and M (number of) Maxwell element branches assembled in parallel. If characterizing the multi-axial material properties using the bulk and shear moduli, the solid like generalized Maxwell model is plotted in Fig. 3, in which K_m and G_m ($m = 1, 2, \cdots M$) are the spring bulk and shear moduli of the *m-th* Maxwell branch, and η_m^K η_m^G are the bulk and shear components of the dashpot viscosity of the *m-th* Maxwell branch. If the temperature of interest (*T*) differs from the reference temperature (T_R), the viscosity of the dashpot complies with the time-temperature superposition principle and one has $\eta_m^K(T) = a_T \eta_m^K(T_R)$ and $\eta_m^G(T) = a_T \eta_m^G(T_R)$, where a_T is the time-temperature shift factor.

The stress and strain are analyzed based on the mechanical analogs of the solid-like generalized Maxwell model in Fig 3. The total stress is the sum of the stress in the single spring and the stresses in all Maxwell branches, while the strain remains the same between the single spring and the Maxwell branches. Thus

$$\sigma_{ij} = \sigma_{ij}^{\infty} + \sum_{m=1}^{M} \sigma_{ij}^{m} \tag{18}$$

$$\varepsilon_{ij} = \varepsilon_{ij}^{\infty} = \varepsilon_{ij}^{m} = \varepsilon_{ij}^{m\cdot el} + \varepsilon_{ij}^{m\cdot vi} \tag{19}$$

where σ_{ij}^{∞} and $\varepsilon_{ij}^{\infty}$ are the stress and strain of the single spring, σ_{ij}^{m} and ε_{ij}^{m} are the stress and strain of the *m-th* Maxwell branch. The constitutive relation for the single spring is modeled by an elastic Hooke's law as below:

$$\sigma_{ij}^{\infty} = \frac{1}{3}\sigma_{kk}^{\infty}\delta_{ij} + s_{ij}^{\infty} = K_{\infty}\varepsilon_{kk} + 2G_{\infty}e_{ij} \tag{20}$$

For each Maxwell branch, the strain is decomposed into the elastic strain ($\varepsilon_{ij}^{m\cdot el}$) due to the spring and the viscous strain ($\varepsilon_{ij}^{m\cdot vi}$) due to the dashpot as in Eq. 19. It is noted that the elastic strain or viscous strain between different Maxwell branches can be different since the spring modulus and the dashpot viscosity vary between Maxwell branches. Furthermore, the elastic strain and the viscous strain are decomposed into volumetric and deviatoric components as below:

$$\begin{cases} \varepsilon_{ij}^{m\cdot el} = \dfrac{1}{3}\varepsilon_{kk}^{m\cdot el}\delta_{ij} + e_{ij}^{m\cdot el} \\ \varepsilon_{ij}^{m\cdot vi} = \dfrac{1}{3}\varepsilon_{kk}^{m\cdot vi}\delta_{ij} + e_{ij}^{m\cdot vi} \end{cases} \tag{21}$$

The stress within each Maxwell branch is expressed as the sum of bulk stress and deviatoric stress (i.e., $\sigma_{ij}^{m} = \frac{1}{3}\sigma_{kk}^{m}\delta_{ij} + s_{ij}^{m}$). Since the spring and the dashpot are connected in series in a Maxwell branch, the bulk stress or deviatoric stress of the spring is identical to the bulk stress or deviatoric stress of the dashpot for each Maxwell branch. Therefore,

$$\begin{cases} \sigma_{kk}^{m} = 3K_m\varepsilon_{kk}^{m\cdot el} = 3\eta_m^{K}\dfrac{d\varepsilon_{kk}^{m\cdot vi}}{dt} \\ s_{ij}^{m} = 2G_m e_{ij}^{m\cdot el} = 2\eta_m^{G}\dfrac{de_{ij}^{m\cdot vi}}{dt} \end{cases} \tag{22}$$

Expressing Eq. 19 in terms of bulk strain and deviatoric strain gives $\varepsilon_{kk} = \varepsilon_{kk}^{m\cdot el} + \varepsilon_{kk}^{m\cdot vi}$ and $e_{ij} = e_{ij}^{m\cdot el} + e_{ij}^{m\cdot vi}$. Substituting these two equations and $\eta_m^{K} = a_T K_m \tau_m, \eta_m^{G} = a_T G_m \tau_m$ into Eq. 22 gives:

$$\begin{cases} a_T\tau_m\dfrac{d\varepsilon_{kk}^{m\cdot vi}}{dt} + \varepsilon_{kk}^{m\cdot vi} - \varepsilon_{kk} = 0 \\ a_T\tau_m\dfrac{de_{ij}^{m\cdot vi}}{dt} + e_{ij}^{m\cdot vi} - e_{ij} = 0 \end{cases} \tag{23}$$

For a given strain history (e.g., $\varepsilon_{ij}(t) = \frac{1}{3}\varepsilon_{kk}(t)\delta_{ij} + e_{ij}(t)$), Eq. 23 works as an ordinary differential equation (ODE) which can be used to solve for the viscous strains (i.e., $\varepsilon_{kk}^{m\cdot vi}$ and $e_{ij}^{m\cdot vi}$) provided time boundary conditions are known. Once the viscous strains are solved, the stress for each Maxwell branch is calculated by:

$$\sigma_{ij}^{m} = K_m\left(\varepsilon_{kk} - \varepsilon_{kk}^{m\cdot vi}\right)\delta_{ij} + 2G_m\left(e_{ij} - e_{ij}^{m\cdot vi}\right) \tag{24}$$

The three-dimensional stress-strain constitutive relation for the generalized Maxwell model is obtained by combining Eqs. 18, 20, and 24 and presented as:

$$\sigma_{ij} = K_\infty\varepsilon_{kk} + 2G_\infty e_{ij} + \sum_{m=1}^{M}\left[K_m\left(\varepsilon_{kk} - \varepsilon_{kk}^{m\cdot vi}\right)\delta_{ij} + 2G_m\left(e_{ij} - e_{ij}^{m\cdot vi}\right)\right] \tag{25}$$

Then the solved viscous strains together with the given strain history and the material properties (bulk and shear moduli) are used in Eq. 25 to predict the stress responses due to the given strain history. Thus Eqs. 23 and 25 define the multi-axial constitutive relations for a viscoelastic material and can be easily embedded in a finite element modeling such as in a weak form PDE modeling.

Weak Form PDE Modeling of Viscoelasticity

The weak form of a PDE is an important mathematical analysis method to find the solutions to the PDE. The original form PDE (e.g., Eq. 26) is a strong form which requires the PDE to be satisfied at every point and all terms must be sufficiently continuous for derivatives. However, the PDEs dominating natural physics are not necessarily continuous and some terms in the PDE are only defined over a small region. A weak form PDE provides a better model for these situations. Take a structural analysis as an example, Eq. 26 is the strong form PDE of the Poisson's equation.

$$-\nabla\cdot\left(c\nabla\mathbf{u}\right) = f \tag{26}$$

where $\nabla\mathbf{u}$ and $\nabla\cdot\mathbf{u}$ are gradient and divergence of a vector **u** such as a displacement vector. *f* is a source, e.g., body force. *c* is a coefficient matrix such as a modulus matrix. Multiplying both sides of Eq. 26 by a test function *v* and integrating the both sides over a region Ω give:

$$\int_{\Omega}\left[-\nabla\cdot\left(c\nabla\mathbf{u}\right)\right]v d\Omega=\int_{\Omega}fv d\Omega \tag{27}$$

If the solution to Eq. 26 is *V* and Eq. 27 holds for any $v\in V$, one can say Eq.27 is equivalent to Eq. 26 in the region Ω. Integrating the left side of Eq. 27 by parts and using the Gauss theorem to convert a body integration to a surface integration and applying a surface traction boundary condition (e.g., $\mathbf{n}\cdot\left(c\nabla\mathbf{u}\right)=P$), one can get:

$$\int_{\Omega}\left[\left(c\nabla\mathbf{u}\right)\cdot\nabla v-fv\right]d\Omega-\int_{\partial\Omega}PvdS=0 \tag{28}$$

where *P* is the surface traction and *S* is the area of the surface of the region Ω, i.e., $\partial\Omega$.

Eq. 28 is the weak form for the strong form PDE in Eq. 26. In fact, the weak form PDE can be regarded as a generalization of the virtual work principle where the test function *v* is equivalent to the virtual displacement. Thus, if let $v=\delta u$ where δu is a small virtual displacement disturbance, one can derive that the left side of Eq. 28 gives the virtual work increment due to the small displacement disturbance. The advantages of using the weak form PDE are 1) lower continuity requirement on the solution compared to the strong form PDE as the weak form reduces the maximum order of the spatial derivatives, e.g., Eq. 26 is a second-order derivative while Eq. 28 is a first-order derivative; 2) the boundary conditions are clearly specified in the weak form PDE, such as the surface integration in Eq. 28. Because of these, a weak form PDE is particularly suitable for discretization and numerical solution using the finite element method.

Comsol Multiphysics provides strong solvers and user-friendly interfaces to find the solutions to any forms of PDEs using weak form modeling. In Comsol PDE modeling, users only need to input *Weak Expressions* which are the integrands of the weak form PDE. Comsol will then perform a numerical integration as $0=\int_{\Omega}\left(Weak\ Expressions\right)d\Omega$. For example, the spatial integrand of Eq. 28 is $\left(c\nabla\mathbf{u}\right)\cdot\nabla v-fv$ which can be rewritten in *Weak Expressions* as

$$-\left\{c*\left[ux*test\left(ux\right)+uy*test\left(uy\right)+uz*test\left(uz\right)\right]-f*\left[test\left(\mathbf{u}\right)\right]\right\} \tag{29}$$

where $v=test\left(\mathbf{u}\right)$ is pre-defined in Comsol (COMSOL 2013a) and $\nabla test\left(\mathbf{u}\right)=test\left(\nabla\mathbf{u}\right)$ is used. *ux*, *uy* and *uz* are spatial derivatives of the vector **u**. The symbol $*$ stands for "multiplied by". A negative sign is added to the weak expressions as the Comsol convention has the integral in the right-hand side of the equation (COMSOL 2013a).

In this study, the viscoelastic modeling is conducted in Comsol using a *Weak Form PDE* module and a *Linear Elastic Solid* module to solve the viscous and elastic responses of the generalized Maxwell model, respectively. It is noted that the existing viscoelastic module in Comsol assumes that the viscous part of the deformation is incompressible and all viscous deformations are attributed to the shear stresses (COMSOL 2013b). Thus the volumetric deformation is purely elastic, which is not the case for most of the geomaterials such as soils, sands and asphalt mixtures.

The viscous bulk and shear strains in Eqs. 23 have as many components as the number of the strain components of a solid deforming problem. Thus the viscous bulk and shear strains are treated as additional degrees of freedom of the problem and can be solved using weak form PDE modeling. Descriptions of the key modeling steps in Comsol are shown as below:

First, define the material properties in Comsol. The material properties including E_∞, E_m, τ_m and υ_0 shown in Table 3 are input as *Parameters*, and a_T is input as a *Variable* that is a function of temperature, e.g., Eq. 3. The temperature can be defined as a *Parameter* too or solved using a thermal analysis of the structure. Then these material properties are converted to bulk and shear modulus components, i.e., K_∞, G_∞, K_m, and G_m using Eqs. 11 and 12.

Second, define *Dependent Variables* in *Weak Form PDE* module. The viscous volumetric and shear strains (i.e., $\varepsilon_{kk}^{m\cdot vi}$ and $e_{ij}^{m\cdot vi}$) are treated as new *Dependent Variables* and input in the *Weak Form PDE* module. It is noted that $m=1,2,\cdots M$ and $ij=11,12,13,22,23,33$. Thus the total number of the

dependent variables for $\varepsilon_{kk}^{m\cdot vi}$ is M that is the number of Maxwell branches. The total number of the dependent variables for $e_{ij}^{m\cdot vi}$ is 6*M. In this study, $u1m$ and $u2mij$ are assigned in the *Weak Form PDE* module as the dependent variables to represent $\varepsilon_{kk}^{m\cdot vi}$ and $e_{ij}^{m\cdot vi}$, respectively.

Third, input the *Weak Expressions* in the *Weak Form PDE* module. In this study, $\varepsilon_{kk}^{m\cdot vi}$ and $e_{ij}^{m\cdot vi}$ are *Dependent Variables* which do not include spatial derivatives as shown in Eq.23. Thus $\left(c\nabla\mathbf{u}\right)\cdot\nabla v=0$. The source function *f* in Eq. 29 is determined as the left side of Eq. 23. Thus the *Weak Expressions* for Eq. 23 are represented as the second term of Eq. 29 (i.e., $f*\left[test\left(\mathbf{u}\right)\right]$), which are

$$\begin{cases}\left(a_T*\tau_m*\left(u1mt\right)+\left(u1m\right)-solid.eelvol\right)*test\left(u1m\right)\\ \left(a_T*\tau_m*\left(u2mijt\right)+\left(u2mij\right)-solid.eeldevij\right)*test\left(u2mij\right)\end{cases} \tag{30}$$

where $m=1,2,\cdots M$, $ij=11,12,13,22,23,33$; $u1mt$ and $u2mijt$ are time derivatives of the dependent variables $u1m$ and $u2mij$, which represent the components of the viscous volumetric and shear strains, respectively. $solid.eelvol$ and $solid.eeldevij$ are elastic volumetric strain and elastic deviatoric strain components in a long term, respectively, which are determined by the *Linear Elastic Solid* module representing the strain responses of the single spring in the generalized Maxwell model.

Fourth and last, update stresses due to viscous responses. Once the viscous strains are determined, the stress for each Maxwell branch can be calculated using Eq. 24 which is expressed in Comsol as:

$$Smij=K_m\left(solid.eelvol-u1m\right)+2G_m\left(solid.eeldevij-u2mij\right) \tag{31}$$

where $Smij$ ($m=1,2,\cdots M$, and $ij=11,12,13,22,23,33$) are defined in *Variable* and expressed using Eq. 31. Then the total stress is updated based on Eq. 25 and expressed in Comsol as:

$$solid.Silij=\sum_{m=1}^{M}Smij \tag{32}$$

where $solid.Silij$ ($ij=11,12,13,22,23,33$) is the initial stress components which are used to represent the stresses due to viscous strains and will be automatically added to the total stresses in Comsol.

Verification and Validation of Equation Based FE Model

The weak form PDE modeling of viscoelasticity in Comsol is verified through comparing the modeling results in Comsol and that in Abaqus using the same material properties and loading configurations. It is further validated by comparing the weak form modeling results with laboratory test results of the asphalt mixtures.

Verification by Comparing with Abaqus Viscoelastic Simulations

The simulations in both Comsol and Abaqus platforms are performed based on identical material properties and loading configurations. The responding strains are computed by weak form PDE modeling of viscoelasticity in Comsol and by the viscoelastic module in Abaqus. The simulated sample is an axisymmetric cylinder with 100 mm diameter and 200 mm height. The material properties are determined based on one of the tested asphalt mixtures (i.e., the one with 4% air void content and 6 month aging in Table 3). The material properties input in Comsol are E_∞, E_m, τ_m and υ_0, which are directly obtained from Table 3. According to the user's manual (ABAQUS 2010), the material properties input in Abaqus include E_∞, υ_0 which are used as long-term elastic modulus and Poisson's ratio, and g_i, k_i, and τ_i for the Prony viscoelastic model, where $g_i = k_i = E_i \Big/ \left(E_\infty + \sum_{i=1}^{M} E_i \right)$ and $\tau_i = \tau_m$ in which $i, m = 1, 2, \cdots M$. The simulation tests are performed at the reference temperature, thus $a_T = 1$ for both platforms.

The first simulation is a creep and recovery test with confinement. In both platforms, the same loading configurations are applied on the sample: a hydrostatic confining pressure of 100 kPa is applied for 80 s; and a deviatoric stress is ramped up to 200 kPa in 1 s and kept constant for the first 30 s and then unloaded to zero within 1 s and maintained at zero until 80 s. Fig. 4 compares the axial and radial strains determined by the two platforms in a stress/strain vs. log (time) coordinate. It is found that the strains predicted by the two platforms matched well with each other (relative error < 0.1% at each calculation point) in every stage of the test including loading ramp, creep, unloading, and recovery.

The second simulation is a cyclic load test with confinement. In both platforms, the same loading configurations are applied on the sample: a hydrostatic confining pressure of 100 kPa is applied; and a deviatoric cyclic stress is loaded at a frequency of 0.05 Hz with an amplitude of 200 kPa. The test is terminated at 100 s (5 cycles). Fig. 5 shows the stresses and strains with loading time which also match well between the simulation results of the two platforms (relative error < 0.1% at each calculation point). Figs 4 and 5 verify the consistency and accuracy of the weak form PDE-based modeling of viscoelasticity in Comsol, which can produce identical results with other finite element modeling platforms providing all simulation conditions remain the same.

It is noted that, at the same data acquisition rate, both Comsol weak form PDE-based viscoelastic modeling and Abaqus embedded viscoelastic modeling can complete the two simulations within reasonable computational time (i.e., approximately, Comsol used 2 minutes and Abaqus used 1 minute). However, once further mechanisms such as plasticity, fracture, and damage are coupled with viscoelasticity in Abaqus, the existing embedded Abaqus viscoelastic module will not be workable and user-defined programming is needed for the coupled constitutive modeling. In contrast, the PDE-based modeling in Comsol will remain workable and compatible with PDE-based modeling of the other mechanisms, which will be presented in future publications. It must be emphasized that the time and effort required for Comsol programing based on user-interface inputs is super less than that required for Abaqus user-defined programing based on computer coding languages such as FORTRAN or C. Further evaluations of the computational efficiency for PDE-based FE modeling on coupled mechanisms are being performed for a complex material.

Validation by Comparing with Laboratory Results

More validations of the weak form PDE modeling of viscoelasticity are performed by comparing the simulation results with the laboratory test results. Table 1 lists the lab tests that are used in validation including 1) creep tests at three temperatures and 2) cyclic load tests. The loading parameters are also shown in Table 1. Axial strains in the two validation tests were recorded for the six types of asphalt mixtures which are compared with the viscoelastic predictions based on the weak form PDE-FE

simulations in Comsol. The material properties such as relaxation modulus and time-temperature shift factor used as inputs to the FE simulations are determined based on the dynamic modulus tests on the same mixtures, which are shown in Table 3.

Figs. 6-11 show the comparisons between the weak form PDE-FE predictions and the laboratory results of the creep tests at three temperatures for the six asphalt mixtures with two air void contents and three ageing periods, respectively. In the figures, the curves with the legend of "Test Max" and "Test Min" indicate that the strain curves are the maximum and minimum measurements of the three replicates at one temperature, respectively. It is found from the comparisons for all of the six types of the asphalt mixtures that the predicted strains substantially match with the measurements of the lab tests. It is noted that a lower static stress was applied at a higher temperature as shown in Table 1, thus the strain measured at a higher temperature can be less than that at a lower temperature (e.g., the strain at 40°C is less than that at 25°C in Figs. 8, 10, and 11).

Figs. 12-17 show the comparison between the weak form PDE-FE predictions and the laboratory results of the cyclic load tests for the six asphalt mixtures with two air void contents and three ageing periods, respectively. In the figures, the measured total strains are decomposed into static strain and cyclic strain. The static strain is a mean strain based on which the total strain oscillates and the cyclic strain is the oscillation part of the total strain. Thus, the total strain is the sum of the static strain and the cyclic strain. It is found, from the comparisons for the six types of the asphalt mixtures, that the laboratory measured total strain is greater than the weak form PDE-FE predicted total strain. The possible reasons could be 1) a higher stress was used in the cyclic validation test than the dynamic modulus tests whose results were employed to determine the material properties as the FE inputs. Thus the nonlinear viscoelastic responses due to the higher stress were not be captured by the linear viscoelastic model used in the FE modeling; 2) some amount of plastic deformation might be introduced into the sample which was not represented in the FE modeling. It must be noted that the nonlinear viscoelasticity, plastic deformation and viscoplastic deformation can also be modeled by weak form PDE method, which have been achieved in the authors' current work and will be presented in future publications.

Nevertheless, the cyclic strains remain almost identical within each load cycle between the measured and the predicted ones for all of the six types of the asphalt mixtures, as illustrated in Figs. 12-17. The dynamic modulus and phase angle were calculated based on the cyclic strains predicted by the weak form PDE-FE modeling and measured by the laboratory tests, respectively. As illustrated in Fig. 18, the dynamic modulus and phase angle are found to be comparable and matched well between the laboratory measurements and the PDE modeling predictions. This finding validates the accuracy of the viscoelastic modeling using the weak form PDE modeling in the FE program. In sum, Figs. 6-18 demonstrate that the weak form PDE-based viscoelastic modeling can reliably predict the responses of the viscoelastic material such as the asphalt mixtures. It can also be concluded from the comparisons that the viscoelastic material properties determined from dynamic modulus tests and master curves basically provide accurate model inputs for the viscoelastic simulations in the FE modeling.

Summary and Conclusions

The constitutive behavior of viscoelastic materials (asphalt mixtures were taken as examples) was modeled by a weak form partial differential equation (PDE) based finite element (FE) modeling. A solid-like generalized Maxwell model was used to represent the deformation mechanism of the viscoelastic materials. The viscoelastic stress and strain relations were derived and implemented in weak form PDE modeling in the Comsol Multiphysics program, which was verified by comparing virtual laboratory test simulations with Abaqus viscoelastic simulations. Creep and recovery tests and cyclic loading tests, both with confinements, were simulated in Comsol and Abaqus using the same loading configurations and material property inputs. Both produced the identical results in terms of axial and radial strain responses. The weak form PDE modeling of viscoelasticity was further validated by comparing real laboratory test results with Comsol FE predictions. The material viscoelastic properties such as the Prony series model coefficients for relaxation modulus were determined by converting from dynamic modulus and phase angle master curves that were constructed using dynamic modulus test results. Strains in creep tests at

three temperatures and cyclic load tests were predicted and found to be comparable with the measurements of the real laboratory tests.

It was demonstrated that the weak form PDE based FE modeling can serve as an efficient method to implement new constitutive models and free engineers from user subroutine programming. Specifically, 1) the viscoelastic FE modeling using the weak PDE formulation is applicable for all linear viscoelastic materials, and asphalt mixtures were taken as an example in this study; 2) no user subroutine programming is needed in order to implement a new constitutive model using the weak form PDE method. The users only need to define their variables and input the weak form integrand expressions in the *Weak Form PDE* module interface; 3) the weak form PDE modeling allows the users to focus on material constitutive characterizations, but not to be bothered by the numerical issues such as convergence, iteration technologies, etc.

Recommended future work includes extending the weak form PDE modeling to modeling complicated physics/mechanisms such as nonlinearity, plasticity, fracture, damage, thermal and moisture diffusion and evaluate their coupling and interaction effects. These models are being under performed in the authors' current work and will be presented in future publications.

References

ABAQUS (2010). *Abaqus Analysis User's Manuals*, Hibbit, Karlsson & Sorensen Inc., Pawtucket, Rhode Island.

ARA (2004). "Guide for Mechanistic-Empirical Design of New and Rehabilitated Pavement Structures." *National Cooperative Highway Research Program (NCHRP), Report 1-37A, by Applied Research Associates*, Transportation Research Board, National Research Council, Washington, D.C.

Biligiri, K. P., Kaloush, K., and Uzan, J. (2010). "Evaluation of Asphalt Mixtures' Viscoelastic Properties Using Phase Angle Relationships." *International Journal of Pavement Engineering*, 11(2), 143-152.

COMSOL (2013a). *Comsol Multiphysics Reference Manual, Version 4.3b*, Available at: www.comsol.com.

COMSOL (2013b). *Structural Mechanics Module User's Guide, Version 4.3b*, Available at: www.comsol.com.

Darabi, M. K., Abu Al-Rub, R. K., Masad, E. A., Huang, C.-W., and Little, D. N. (2012). "A Modified Viscoplastic Model to Predict the Permanent Deformation of Asphaltic Materials under Cyclic-Compression Loading at High Temperatures." *International Journal of Plasticity*, 35, 100-134.

Findley, W. N., Lai, J. S., and Onaran, K. (1989). *Creep and Relaxation of Nonlinear Viscoelastic Materials with an Introduction to Linear Viscoelasticity*, Dover Publication, Inc., Mineola, New York.

Francken, L., and Verstraeten, J. (1998). "Interlaboratory Test Program on Complex Modulus and Fatigue." *RILEM Report 17, Bituminous Binders and Mixes*, London, UK, 182-215.

Gibson, N. H., Schwartz, C. W., Schapery, R. A., and Witczak, M. W. (2003). "Viscoelastic, Viscoplastic, and Damage Modeling of Asphalt Concrete in Unconfined Compression." *Transportation Research Record: Journal of the Transportation Research Board*, No. 1860, Transportation Research Board of the National Academies, Washington, DC, 3-15.

Hu, S., and Zhou, F. (2010). "Development of a New Interconversion Tool for Hot Mix Asphalt (Hma) Linear Viscoelastic Functions." *Canadian Journal of Civil Engineering*, 37(8), 1071-1081.

Huang, C. W., Abu Al-Rub, R. K., Masad, E. A., and Little, D. N. (2011). "Three-Dimensional Simulations of Asphalt Pavement Permanent Deformation Using a Nonlinear Viscoelastic and Viscoplastic Model." *Journal of Materials in Civil Engineering*, 23(1), 56-68.

Katicha, S., Flintsch, G., Loulizi, A., and Wang, L. (2008). "Conversion of Testing Frequency to Loading Time Applied to the Mechanistic-Empirical Pavement Design Guide." *Transportation Research Record: Journal of the Transportation Research Board*, No. 2087, Transportation Research Board of the National Academies, Washington, DC, 99-108.

Levenberg, E., and Shah, A. (2008). "Interpretation of Complex Modulus Test Results for Asphalt-Aggregate Mixes." *J. Test. Eval.*, 36(4), 326-334.

Levenberg, E., and Uzan, J. (2004). "Triaxial Small-Strain Viscoelastic-Viscoplastic Modeling of Asphalt Aggregate Mixes." *Mechanics of Time-Dependent Materials*, 8(4), 365-384.

Mun, S., Chehab, G. R., and Kim, Y. R. (2007). "Determination of Time-Domain Viscoelastic Functions Using Optimized Interconversion Techniques." *Road Mater. Pavement Des.*, 8(2), 351-365.

Park, S. W., and Schapery, R. A. (1999). "Methods of Interconversion between Linear Viscoelastic Material Functions. Part I — a Numerical Method Based on Prony Series." *International Journal of Solids and Structures*, 36(11), 1653-1675.

Pellinen, T. K., Bonaquist, R. F., and Witczak, M. W. (2002). "Asphalt Mix Master Curve Construction Using Sigmoidal Fitting Function with Non-Linear Least Squares Optimization." *15th Engineering Mechanics Division Conference*, Columbia University, New York, United States.

TxDOT (2004). "Standard Specifications for Construction and Maintenance of Highways, Streets, and Bridges." Texas Department of Transportation, Austin, TX.

TxDOT (2008). "Test Procedure for Design of Bituminous Mixtures." *TxDOT Designation: Tex-204-F*, Texas Department of Transportation, Austin, TX.

Wineman, A. S., and Rajagopal, K. R. (2001). *Mechanical Response of Polymers, an Introduction*, Cambridge University Press, New York, NY.

Witczak, M. W., Kaloush, K., Pellinen, T., and El-Basyouny, M. (2002). "Simple Performance Test for Superpave Mix Design." *National Cooperative Highway Research Program (NCHRP) Report 465*, Transportation Research Board, National Research Council, Washington, D.C.

Zhang, Y., Luo, R., and Lytton, R. L. (2014). "Anisotropic Characterization of Crack Growth in Tertiary Flow of Asphalt Mixtures in Compression." *Journal of Engineering Mechanics*, 140(6), in press.

Zhang, Y., Luo, R., and Lytton, R. L. (2012a). "Anisotropic Viscoelastic Properties of Undamaged Asphalt Mixtures." *Journal of Transportation Engineering*, 138(1), 75-89.

Zhang, Y., Luo, R., and Lytton, R. L. (2012b). "Characterizing Permanent Deformation and Fracture of Asphalt Mixtures by Using Compressive Dynamic Modulus Tests." *Journal of Materials in Civil Engineering*, 24(7), 898-906.

Zhao, Y., Liu, H., Bai, L., and Tan, Y. (2013). "Characterization of Linear Viscoelastic Behavior of Asphalt Concrete Using Complex Modulus Model." *Journal of Materials in Civil Engineering*, 25(10), 1543-1548.

Zhao, Y., Tang, J., and Liu, H. (2012). "Construction of Triaxial Dynamic Modulus Master Curve for Asphalt Mixtures." *Construction and Building Materials*, 37(12), 21-26.

Zhu, H., and Sun, L. (2013). "Mechanistic Rutting Prediction Using a Two-Stage Viscoelastic-Viscoplastic Damage Constitutive Model of Asphalt Mixtures." *Journal of Engineering Mechanics*, 139(11), 1577-1591.

List of Tables

Table 1 Testing materials, protocol and parameters for asphalt concrete.

Asphalt Mixtures	Test Methods	Temperatures	Loading Parameters	Results Obtained	Purpose of Tests
Binder: NuStar (PG67-22) Air Void: 4% and 7% Aging Periods at 60°C for: 0, 3, 6 months (*Note: in* Loading Parameters *column, 0-4% stands for the mixtures with 0-month aging and 4% air void content, and similar notation for the rests*)	Dynamic modulus tests	10°C 25°C 40°C 55°C	25 Hz 10 Hz 5 Hz 1 Hz 0.5 Hz 0.1 Hz	Dynamic modulus; Phase angle	Determination of viscoelastic model parameters
	Compressive creep tests	10°C	300 kPa (0-4%) 200 kPa (0-7%) 500 kPa (3-4%) 400 kPa (3-7%) 500 kPa (6-4%) 500 kPa (6-7%)	Axial strains vs. loading time	Validation of equation based FE modeling of viscoelasticity
		25°C	60 kPa (0-4%) 40 kPa (0-7%) 120 kPa (3-4%) 80 kPa (3-7%) 200 kPa (6-4%) 120 kPa (6-7%)		
		40°C	20 kPa (0-4%) 20 kPa (0-7%) 30 kPa for rests		
	Cyclic load tests	40°C	55 kPa (0-4%) 50 kPa (0-7%) 65 kPa (3-4%) 60 kPa (3-7%) 80 kPa (6-4%) 65 kPa (6-7%) All at 1 Hz	Axial strains vs. loading cycles	

Table 2 Master curve model coefficients of dynamic moduli and phase angles and corresponding time-temperature shift factor model coefficients for the six different asphalt mixtures

Binder		NuStar Binder (PG67-22)					
Aging Periods		0 month		3 months		6 months	
Air Void Contents		4%	7%	4%	7%	4%	7%
Master Curve Coefficients for |E*| (MPa)	δ	1.254	0.756	1.562	1.195	1.583	1.533
	α	3.381	3.723	3.028	3.259	3.082	2.995
	η	-0.345	-0.203	-0.361	-0.483	-0.560	-0.381
	γ	0.486	0.424	0.508	0.463	0.432	0.469
a_T for |E*|	a	0.0001	0.0001	0.0001	0.0001	0.0001	0.0001
	b	-0.193	-0.160	-0.170	-0.171	-0.194	-0.184
	c	50.62	40.17	43.32	43.85	51.09	47.77
Master Curve Coefficients for φ(°)	φ_{max}	31.9	32.4	32.2	33.5	32.3	31.7
	f_0	0.2016	0.6557	0.1146	0.0563	0.0371	0.1212
	β	0.0187	0.0277	0.0255	0.0225	0.0220	0.0241
a_T for φ	a	0.0010	0.0011	0.0010	0.0011	0.0010	0.0010
	b	-0.712	-0.746	-0.683	-0.739	-0.706	-0.714
	c	125.0	125.7	115.8	123.4	123.1	125.6

Table 3 Coefficients of relaxation modulus Prony series model determined using dynamic modulus and phase angle master curves and Poisson's ratio for the six type asphalt mixtures

Binder		NuStar Binder (PG67-22)						Relaxation	
Aging Periods		0 month		3 months		6 months		Time For All	
Air Void Contents		4%	7%	4%	7%	4%	7%	Mixtures	
Long-term Modulus	E_∞	41.1	10.4	28.1	71.9	67.2	50.9	τ_m (s)	
E_m (MPa)	E_1	3093.4	2985.5	3994.6	2368.7	3602.2	2426.9	τ_1	1.0E-06
	E_2	6040.0	2498.9	5484.8	2494.2	4548.6	2909.8	τ_2	1.0E-05
	E_3	6994.3	2227.8	5026.8	3481.2	5584.0	4004.5	τ_3	1.0E-04
	E_4	5565.7	1120.2	3843.1	3547.0	5849.0	4572.9	τ_4	1.0E-03
	E_5	3292.7	619.5	1989.0	2565.3	4584.5	3132.8	τ_5	1.0E-02
	E_6	1649.0	189.1	743.0	1471.7	2848.8	1668.7	τ_6	1.0E-01
	E_7	525.1	75.2	268.5	560.7	1312.5	734.1	τ_7	1.0E+00
	E_8	177.6	29.2	149.4	235.2	570.7	265.3	τ_8	1.0E+01
	E_9	129.7	1.3	45.0	92.0	314.8	183.1	τ_9	1.0E+02
	E_{10}	37.6	16.2	25.0	2.5	94.3	43.6	τ_{10}	1.0E+03
	E_{11}	2.9	28.6	25.9	16.1	29.2	17.1	τ_{11}	1.0E+04
Instantaneous modulus	E(0)	27549.2	9801.8	21623.3	16906.5	29406.0	20009.6	*data were from a previous study (Zhang et al. 2014)	
Poisson's Ratio	υ_0*	0.32	0.34	0.28	0.29	0.10	0.24		

Figure Caption List

Fig. 1. Dynamic moduli at different temperatures and master curves at 40°C (R^2 = 0.9994 for |E*| Master Curve, R^2 = 0.9712 for |E*| Predicted by Prony Series Relaxation Modulus Model)

Fig. 2. Phase angles at different temperatures and master curves at 40°C (R^2 = 0.9930 for Phase Angle Master Curve, R^2 = 0.9712 for Phase Angle Predicted by Prony Series Relaxation Modulus Model)

Fig. 3. Mechanical analogs of solid-like generalized Maxwell model

Fig. 4. Comparison between Comsol weak form PDE-FE modeling and Abaqus modeling of a viscoelastic material (e.g., asphalt mixture) in a creep and recovery test with confinement (note: loading time was plotted in the log-scale to clearly show the predictions during loading and unloading transitions)

Fig. 5. Comparison between Comsol weak form PDE-FE modeling and Abaqus modeling of a viscoelastic material (e.g., asphalt mixture) in a cyclic loading test with confinement

Fig. 6. Comparison between weak form PDE-FE model predictions and laboratory results of creep tests on asphalt mixtures (4% air void and 0-month aged) at three temperatures

Fig. 7. Comparison between weak form PDE-FE model predictions and laboratory results of creep tests on asphalt mixtures (7% air void and 0-month aged) at three temperatures

Fig. 8. Comparison between weak form PDE-FE model predictions and laboratory results of creep tests on asphalt mixtures (4% air void and 3-month aged) at three temperatures

Fig. 9. Comparison between weak form PDE-FE model predictions and laboratory results of creep tests on asphalt mixtures (7% air void and 3-month aged) at three temperatures

Fig. 10. Comparison between weak form PDE-FE model predictions and laboratory results of creep tests for asphalt mixtures (4% air void and 6-month aged) at three temperatures

Fig. 11. Comparison between weak form PDE-FE model predictions and laboratory results of creep tests on asphalt mixtures (7% air void and 6-month aged) at three temperatures

Fig. 12. Comparison between weak form PDE-FE model predictions and laboratory results of cyclic loading test on asphalt mixtures (4% air void and 0-month aged) (Note: Total strain is decomposed into static strain and cyclic strain, and the same for Figs. 13-17)

Fig. 13. Comparison between weak form PDE-FE model predictions and laboratory results of cyclic loading test on asphalt mixtures (7% air void and 0-month aged)

Fig. 14. Comparison between weak form PDE-FE model predictions and laboratory results of cyclic loading test on asphalt mixtures (4% air void and 3-month aged)

Fig. 15. Comparison between weak form PDE-FE model predictions and laboratory results of cyclic loading test on asphalt mixtures (7% air void and 3-month aged)

Fig. 16. Comparison between weak form PDE-FE model predictions and laboratory results of a cyclic loading test on asphalt mixtures (4% air void and 6-month aged)

Fig. 17. Comparison between weak form PDE-FE model predictions and laboratory results of cyclic loading test on asphalt mixtures (7% air void and 6-month aged)

Fig. 18. Comparisons for dynamic moduli and phase angles predicted by weak form PDE-FE modeling and measured by the laboratory tests for six type asphalt mixtures (E* is dynamic modulus, ϕ is phase angle, 4% stands for air void content and 0-m stands for 0-month aged asphalt mixture)

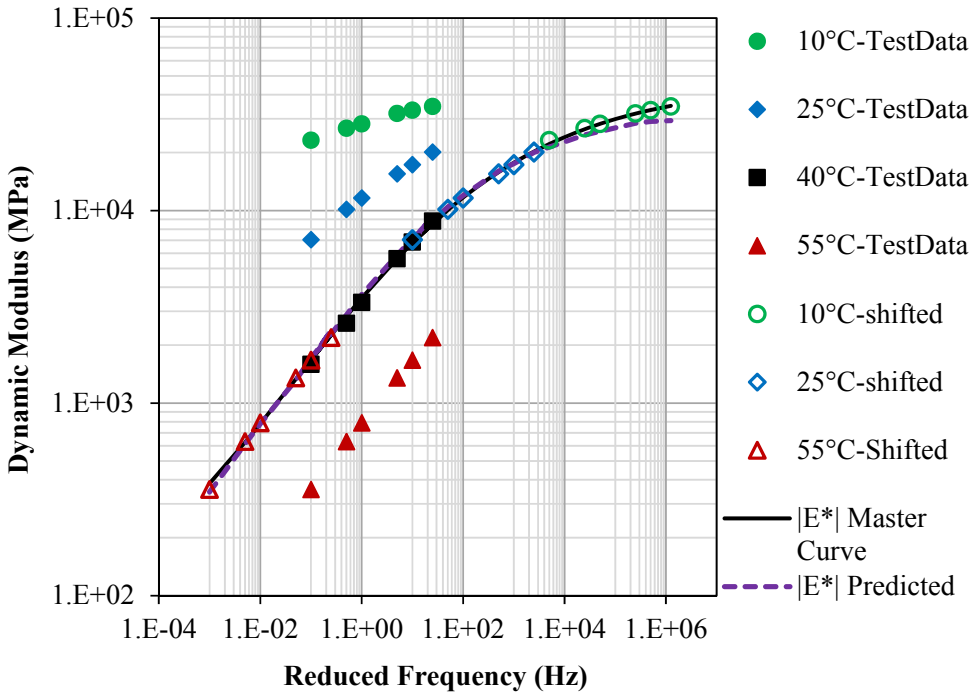

Fig. 1. Dynamic moduli at different temperatures and master curves at 40°C (R^2 = 0.9994 for |E*| Master Curve, R^2 = 0.9712 for |E*| Predicted by Prony Series Relaxation Modulus Model)

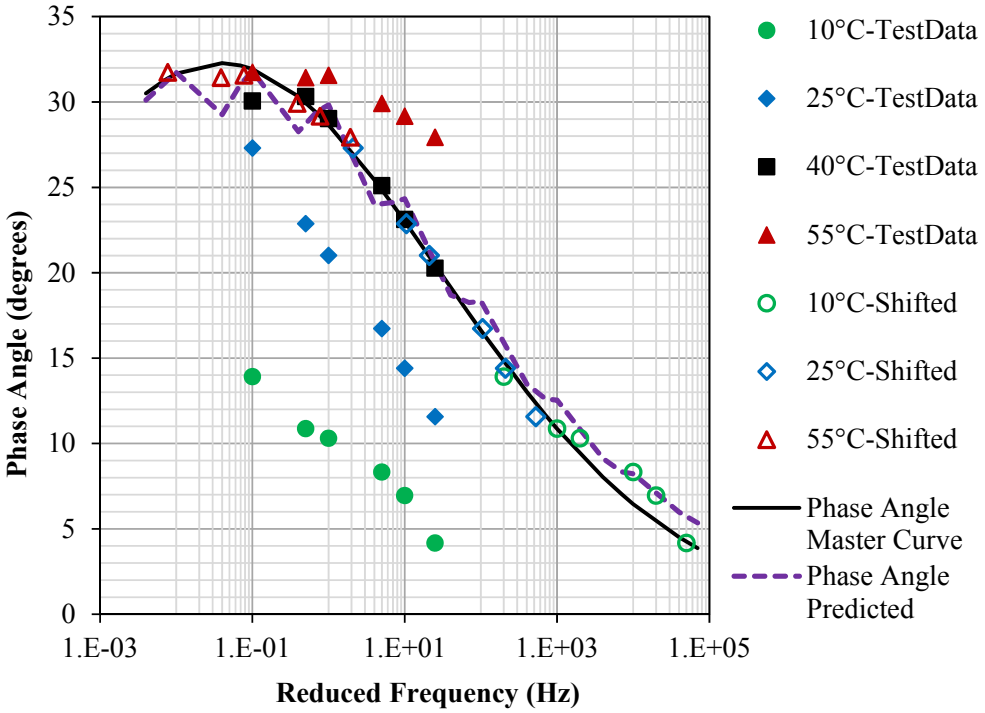

Fig. 2. Phase angles at different temperatures and master curves at 40°C (R^2 = 0.9930 for Phase Angle Master Curve, R^2 = 0.9712 for Phase Angle Predicted by Prony Series Relaxation Modulus Model)

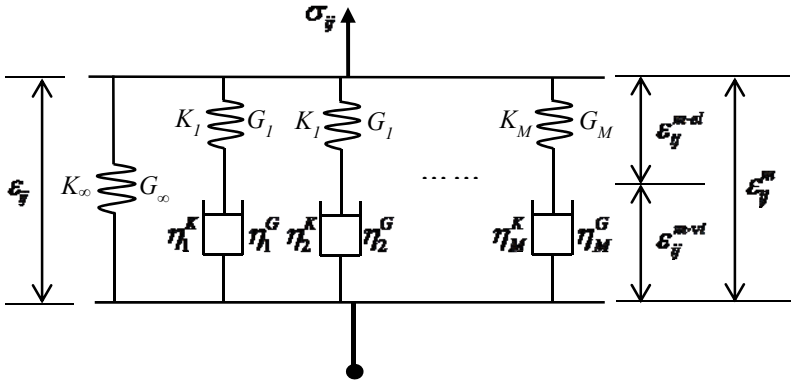

Fig. 3. Mechanical analogs of solid-like generalized Maxwell model

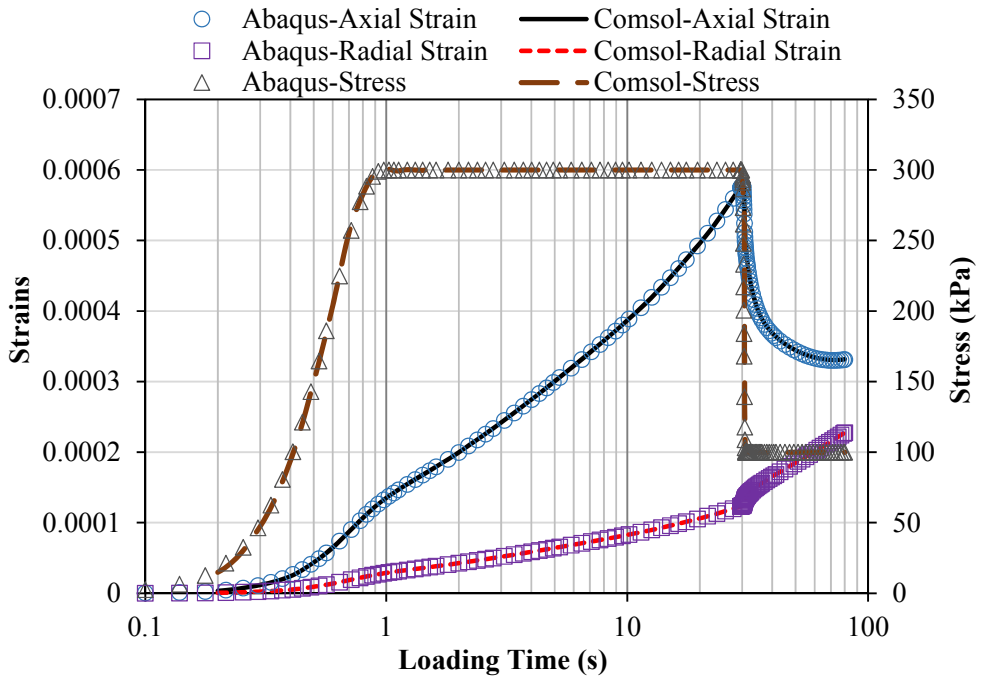

Fig. 4. Comparison between Comsol weak form PDE-FE modeling and Abaqus modeling of a viscoelastic material (e.g., asphalt mixture) in a creep and recovery test with confinement (note: loading time was plotted in the log-scale to clearly show the predictions during loading and unloading transitions)

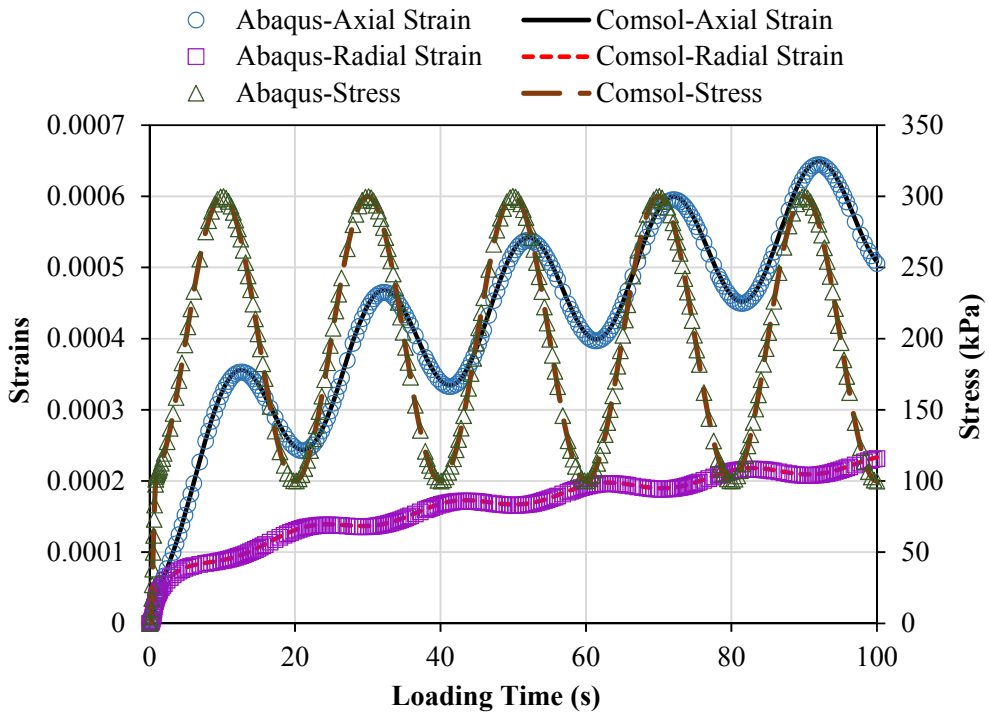

Fig. 5. Comparison between Comsol weak form PDE-FE modeling and Abaqus modeling of a viscoelastic material (e.g., asphalt mixture) in a cyclic loading test with confinement

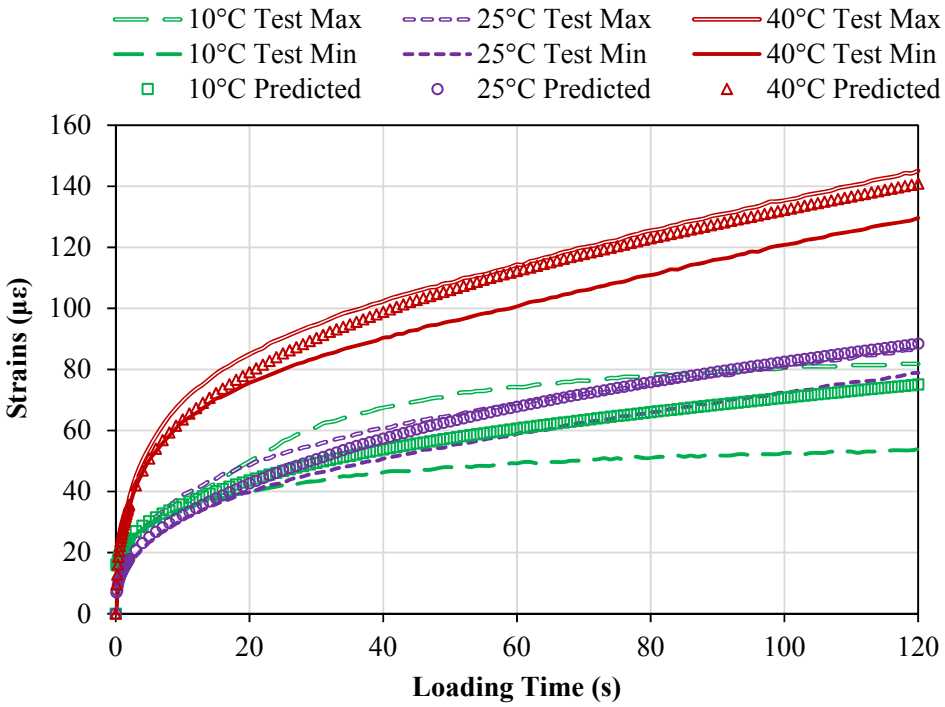

Fig. 6. Comparison between weak form PDE-FE model predictions and laboratory results of creep tests on asphalt mixtures (4% air void and 0-month aged) at three temperatures

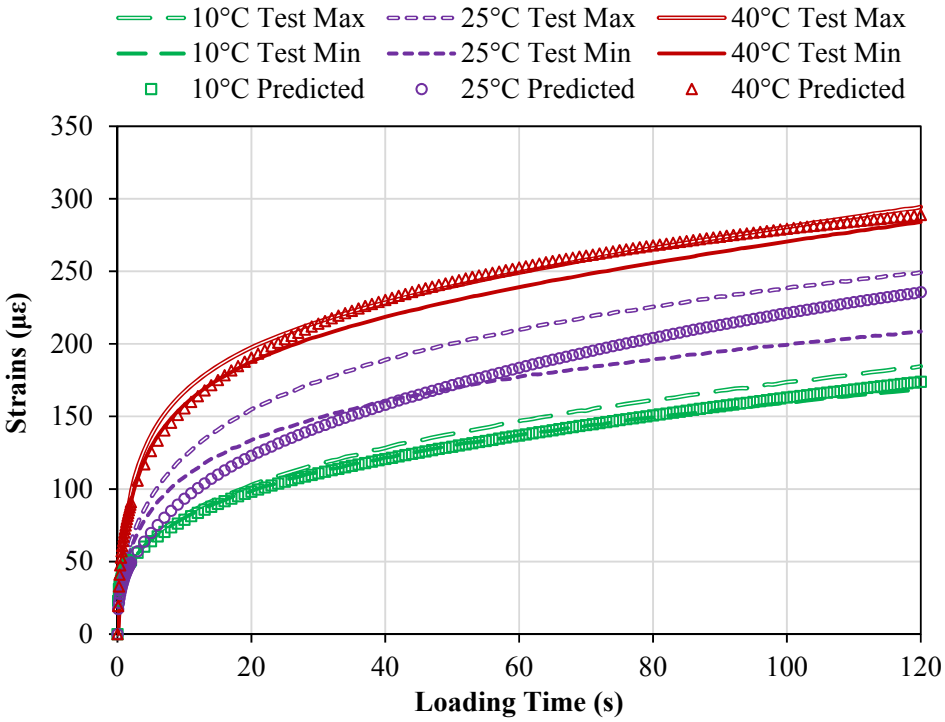

Fig. 7. Comparison between weak form PDE-FE model predictions and laboratory results of creep tests on asphalt mixtures (7% air void and 0-month aged) at three temperatures

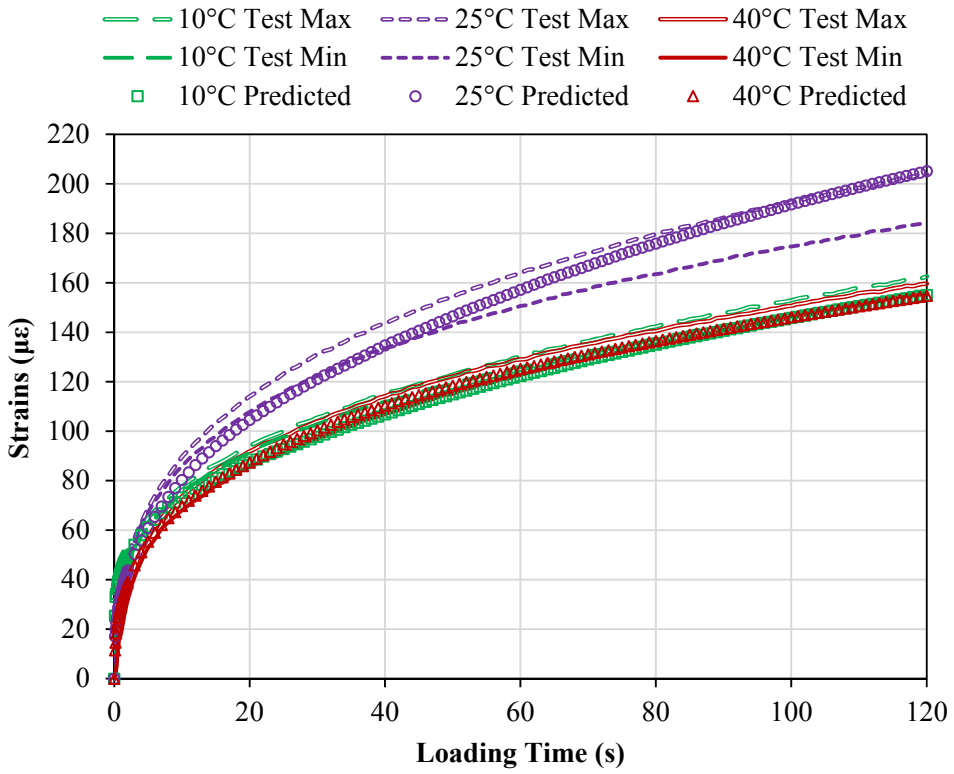

Fig. 8. Comparison between weak form PDE-FE model predictions and laboratory results of creep tests on asphalt mixtures (4% air void and 3-month aged) at three temperatures

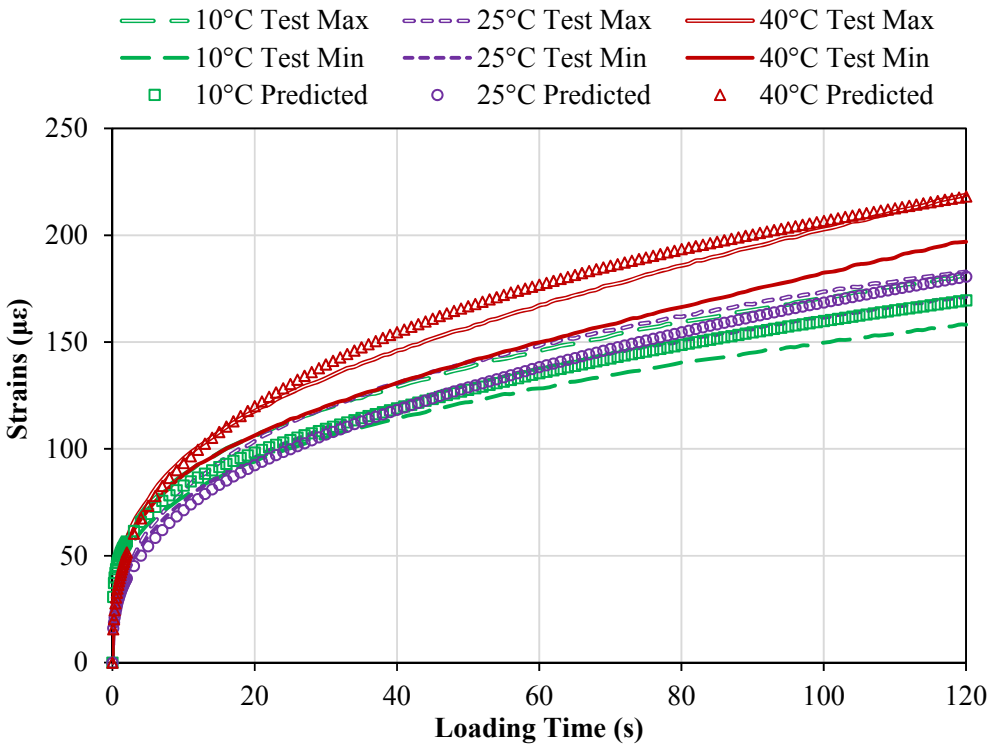

Fig. 9. Comparison between weak form PDE-FE model predictions and laboratory results of creep tests on asphalt mixtures (7% air void and 3-month aged) at three temperatures

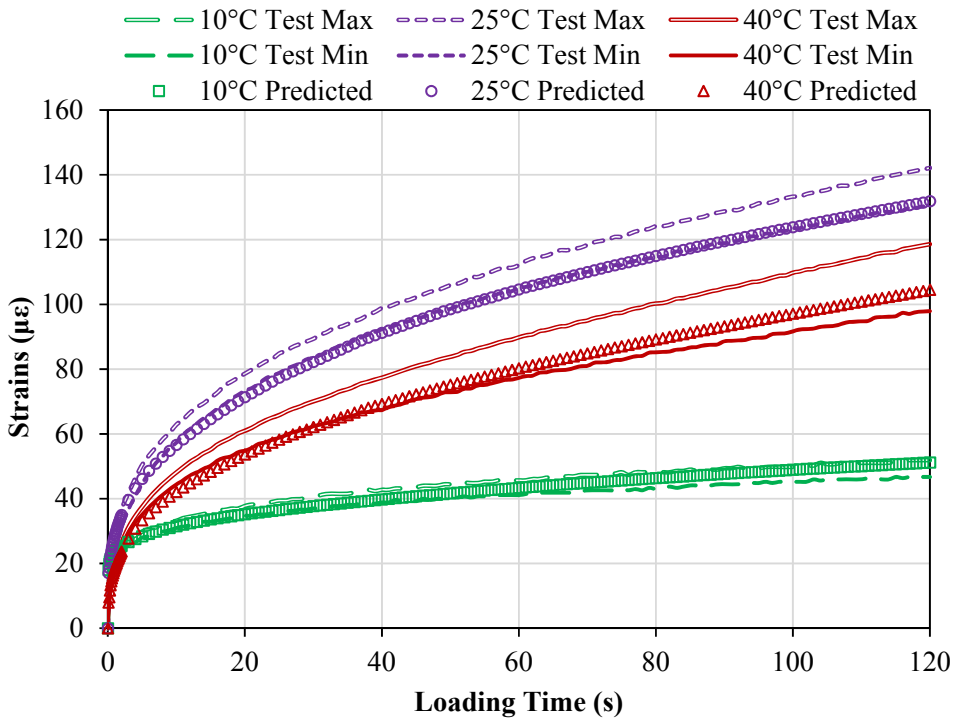

Fig. 10. Comparison between weak form PDE-FE model predictions and laboratory results of creep tests for asphalt mixtures (4% air void and 6-month aged) at three temperatures

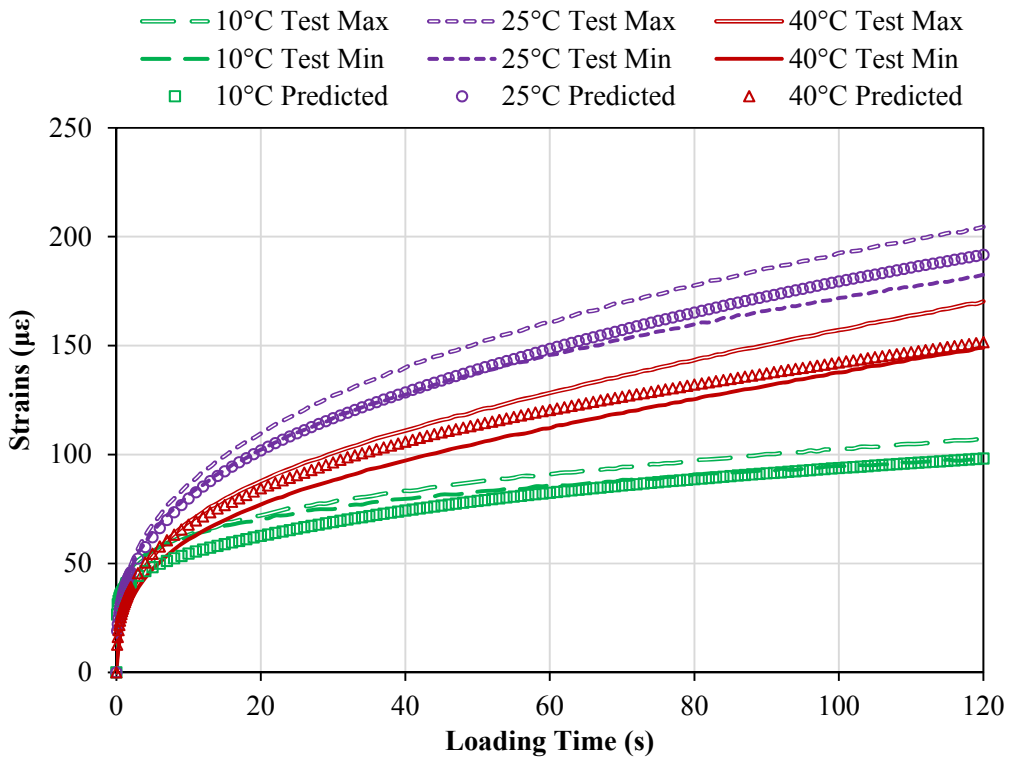

Fig. 11. Comparison between weak form PDE-FE model predictions and laboratory results of creep tests on asphalt mixtures (7% air void and 6-month aged) at three temperatures

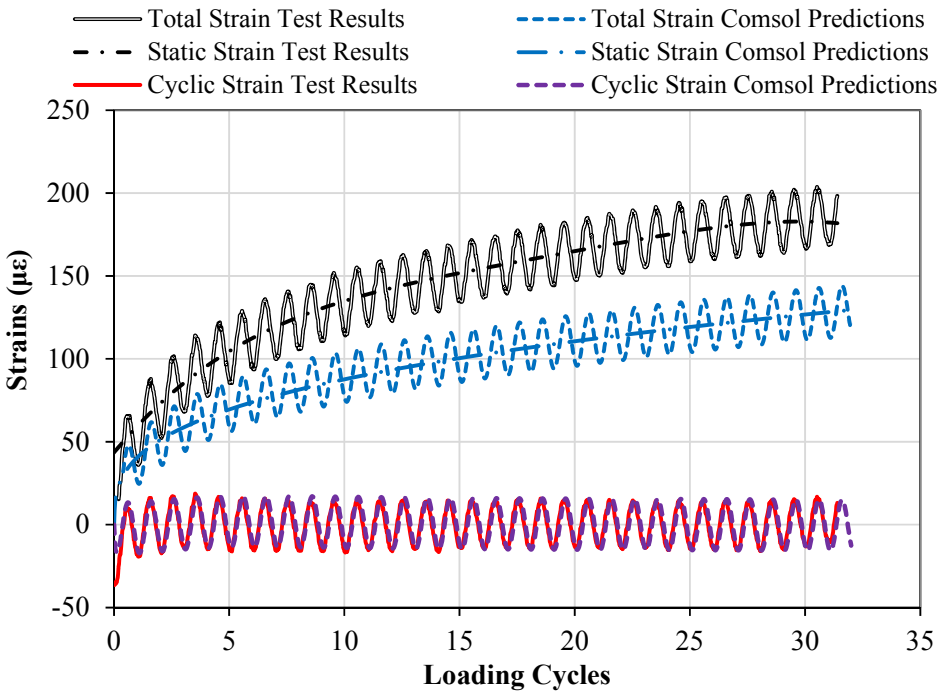

Fig. 12. Comparison between weak form PDE-FE model predictions and laboratory results of cyclic loading test on asphalt mixtures (4% air void and 0-month aged) (Note: Total strain is decomposed into static strain and cyclic strain, and the same for Figs. 13-17)

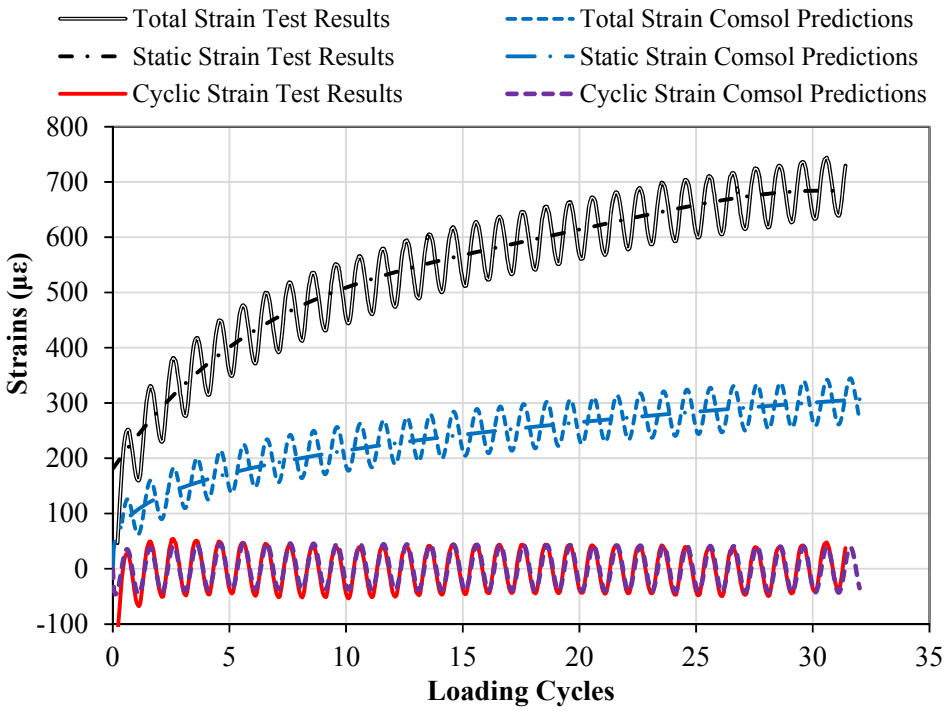

Fig. 13. Comparison between weak form PDE-FE model predictions and laboratory results of cyclic loading test on asphalt mixtures (7% air void and 0-month aged)

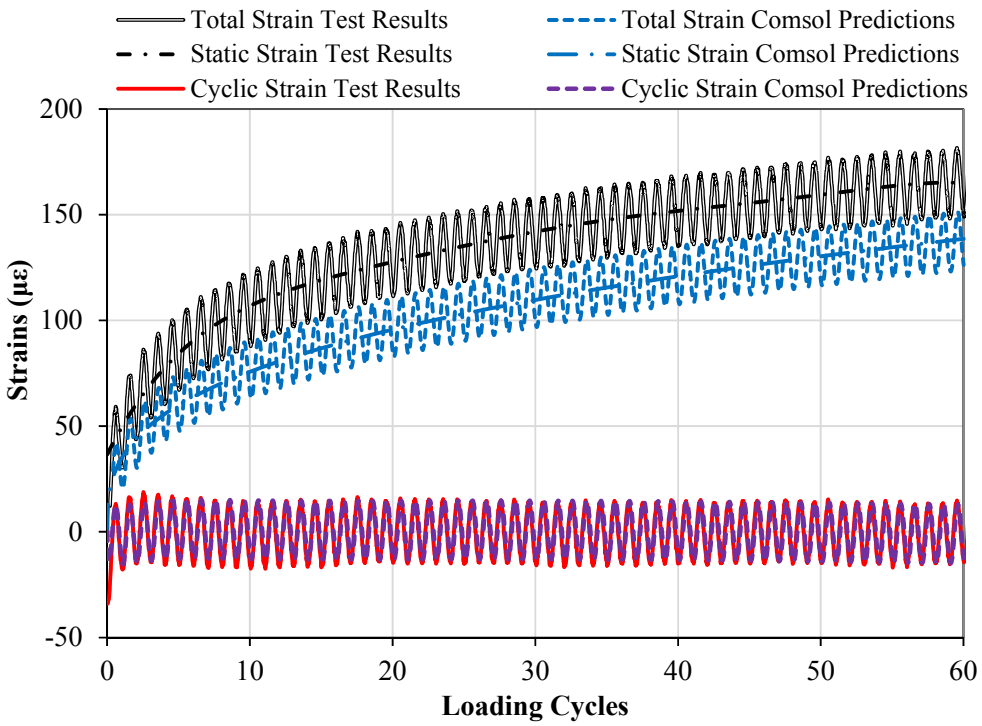

Fig. 14. Comparison between weak form PDE-FE model predictions and laboratory results of cyclic loading test on asphalt mixtures (4% air void and 3-month aged)

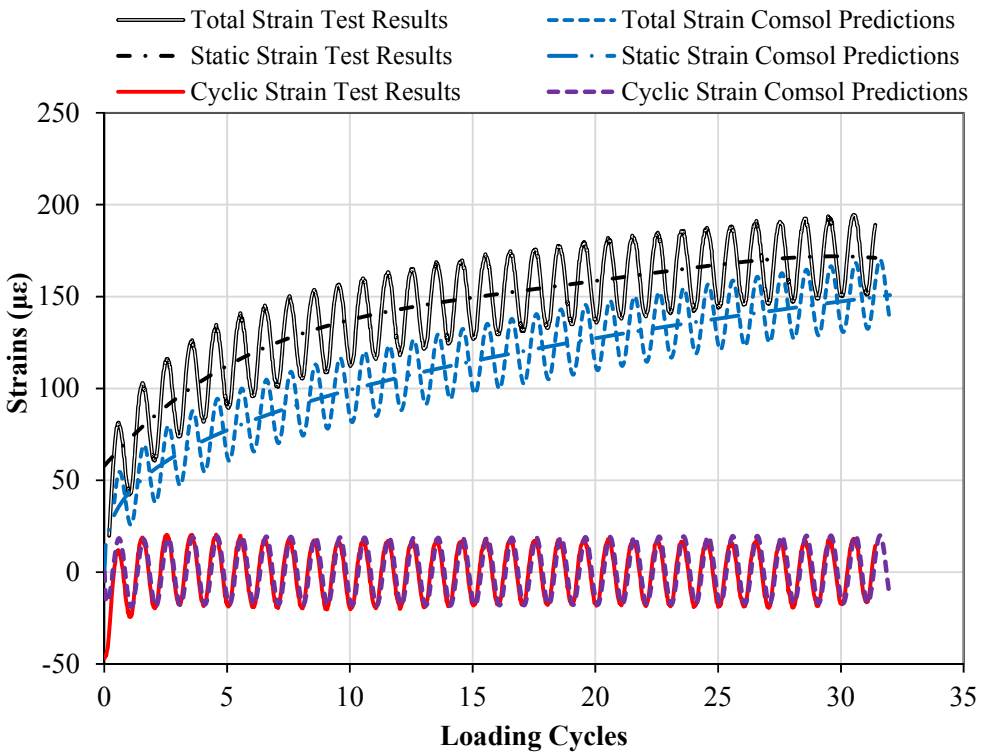

Fig. 15. Comparison between weak form PDE-FE model predictions and laboratory results of cyclic loading test on asphalt mixtures (7% air void and 3-month aged)

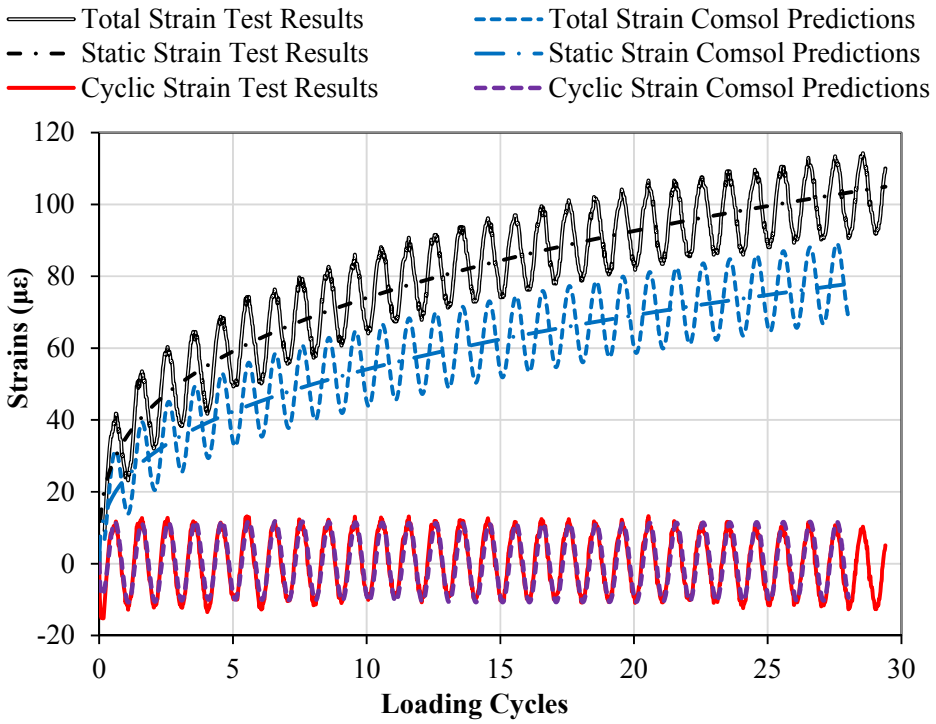

Fig. 16. Comparison between weak form PDE-FE model predictions and laboratory results of a cyclic loading test on asphalt mixtures (4% air void and 6-month aged)

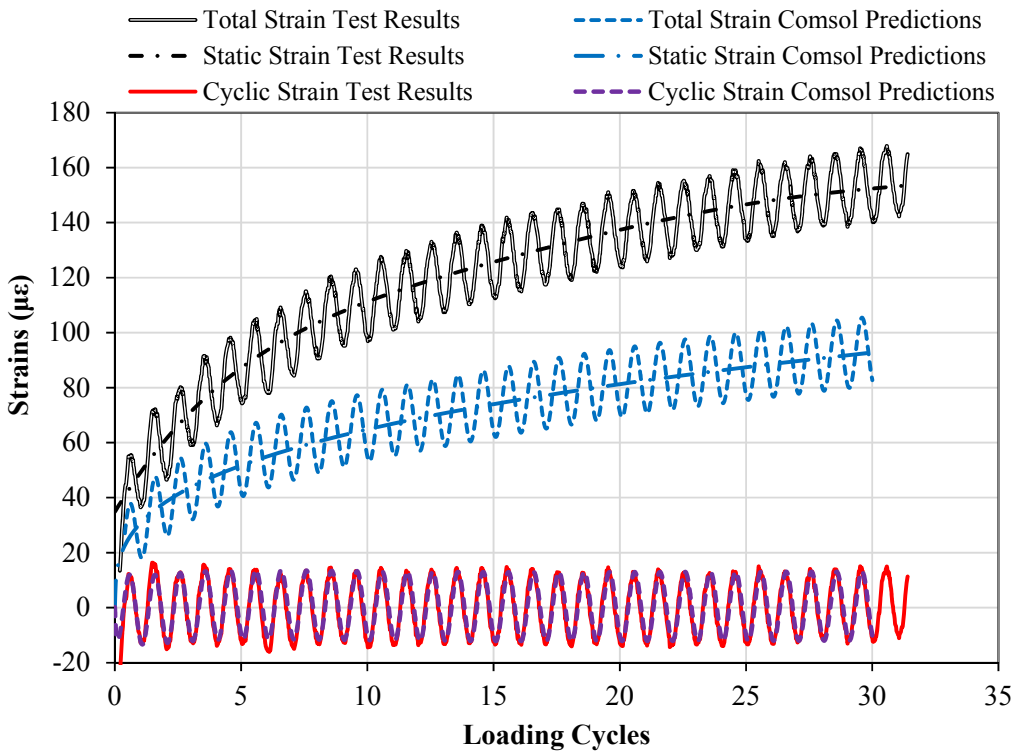

Fig. 17. Comparison between weak form PDE-FE model predictions and laboratory results of cyclic loading test on asphalt mixtures (7% air void and 6-month aged)

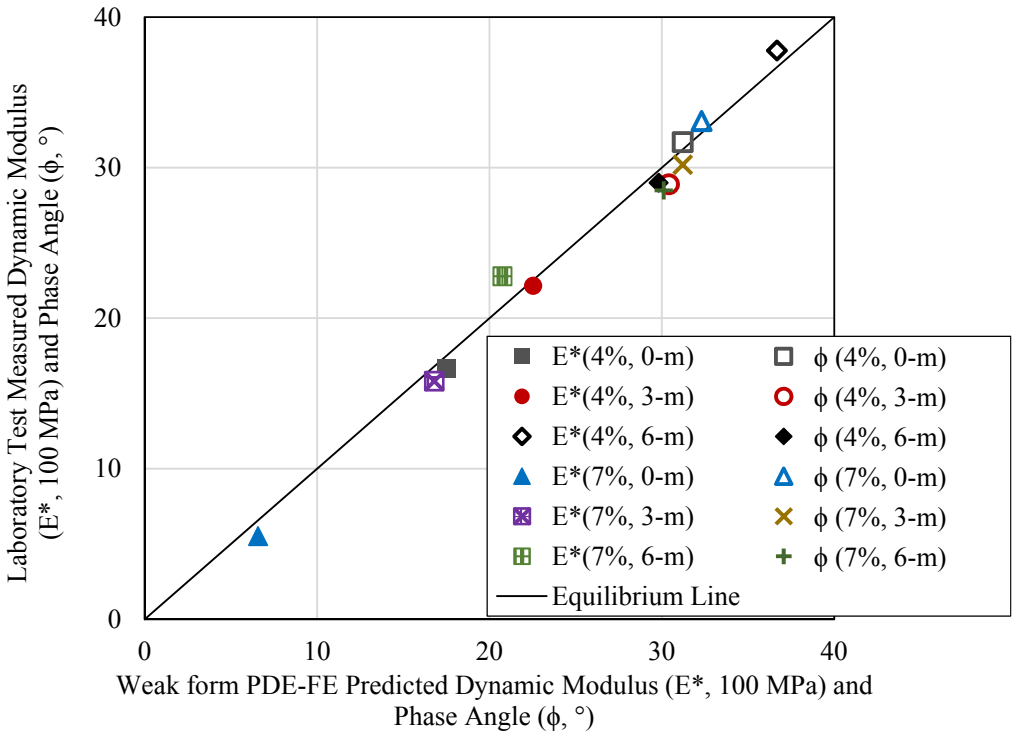

Fig. 18. Comparisons for dynamic moduli and phase angles predicted by weak form PDE-FE modeling and measured by the laboratory tests for six type asphalt mixtures (E* is dynamic modulus, ϕ is phase angle, 4% stands for air void content and 0-m stands for 0-month aged asphalt mixture)